Corrosion Behavior of Cu–Al–Ni–xCo Shape Memory Alloys Coupled with Low-Carbon Steel for Civil Engineering Applications

Abdillah Sani M. Najib[1] · Safaa N. Saud[2] · Esah Hamzah[1]

Abstract

Due to the promising mechanical properties of Cu-based shape memory alloys (SMAs), their applications have become essential in many applications. In the present study, the galvanic behaviors of coupled and uncoupled steel bars with Cu–Al–Ni–xCo shape memory alloys were investigated in 3.5% NaCl solution. Thirteen measurement cells were considered for coupled and uncoupled steels and aged/unaged Cu–Al–Ni–xCo shape memory alloys. The electrochemical measurements were carried out three times to ensure the consistency of the corrosion behavior after the samples were immersed in 3.5% NaCl solution. The results revealed that the addition of 1 wt% Cobalt followed by an aging treatment led to an improvement in the corrosion resistance of coupled steel/Cu–Al–Ni–xCo shape memory alloys and a reduction in the corrosion rate by 50% for the steel bars.

Keywords Corrosion · Coupled steel/Cu–Al–Ni–xCo shape memory alloys · Galvanic behavior · Aging

1 Introduction

Nowadays, researchers have increased their interest in smart material applications, as this promising method can meet the technological demands in various industries. A smart material is a material which reacts to a stimulus or environmental change [1, 2]. Shape memory alloys (SMAs) are regarded as smart materials, as they exhibit physical recovery to their original shapes after being deformed upon heating to critical temperatures [3–5]. There are two phases in shape memory alloys that govern the shape memory effect (SME). These phases have different crystal structures and therefore have their own different properties. At high temperatures, shape memory alloys are in a phase called austenite (A), which exhibits cubic crystals, whereas, at low temperatures, shape memory alloys are in the martensite (M) phase, which can involve tetragonal, orthorhombic, or monoclinic crystals. The structural

transformation between the two phases can occur via lattice distortion instead of diffusion, in which case, this transformation is denoted the martensitic transformation. Each martensitic crystal has an orientation direction referred to as its variant. Assemblies of martensitic variants exist in two forms, i.e., either the twinned martensite (M^t) or detwinned/reoriented martensite (M^d) assembly. M^t is formed by a combination of "self-accommodated" martensitic variants and therefore has a random orientation [6, 7]. On the other hand, detwinned martensite M^d has a specific dominant variant. The shape memory effect occurs due to the reversible phase transformation from austenite to martensite and vice versa. When the material is heated into austenite and subsequently cooled to martensite, M^t is predominantly formed. At low temperatures, when a shape memory alloy is subjected to stress, the variants rearrange and coalesce via the intervening boundaries' movement, resulting in macroscopic change. Formation of the most favorably oriented martensite variants (M^d) occurs during the process [8]. When heated, martensite turns back into austenite, changing shape again. Subsequent cooling then would lead to formation of twinned martensite (M^t) again, but this time with no associated shape change [5]. The applications of shape memory alloys are numerous, covering from medicals and utensils to actuators in oil and gas [9]. The Cu–Al–Ni shape memory alloy is known for its

✉ Esah Hamzah
  esah@mail.fkm.utm.my

1 Faculty of Mechanical Engineering, Universiti Teknologi Malaysia, UTM Skudai, 81310 Johor Bahru, Johor, Malaysia

2 Faculty of Information Sciences and Engineering, Management & Science University, 40100 Shah Alam, Selangor, Malaysia

low cost and ability to maintain the shape memory effect at high temperatures [10]. Furthermore, it also has a high damping capacity, to the extent that it exceeded that of the widely used shape memory alloys, Nitinol [11]. These characteristics of Cu–Al–Ni make it suitable for use in actuators, fasteners, bridge-damping elements, buildings, and oil well applications, as well as other components and structures [12]. However, when used in applications, deterioration, such as that produced by erosion and corrosion, must be considered, especially in highly corrosive environments such as coastal areas and on oilrigs. Moreover, it is more practical and affordable to use the shape memory alloys as a part of a component rather than as the whole system in and of itself. However, this situation may introduce galvanic corrosion, as shape memory alloys is in direct contact with other types of metals. Being one of the promising candidate shape memory alloys for application in industry, Cu–Al–Ni has adequate corrosion resistance, as the alumina layer formed acts as a passive film [13]. However, it is also important to note that Cu–Al–Ni alloy suffers a drawback by which it shows some susceptibility to post-quench aging, leading to a change in mechanical properties when it is subjected to very high-temperature service conditions that become more severe as the time of operation increases [14]. Correspondingly, much research has been conducted to improve Cu–Al–Ni's properties in terms of its application range and to meet specific industrial demand. Several techniques have been introduced to enhance the properties of shape memory alloys, and one such technique is referred to as grain refinement, wherein a small amount of quaternary elements, such as zirconium and titanium, are added to the shape memory alloys [15, 16]. The corrosion resistance of Cu–Al–Ni shape memory alloy improves as the grain becomes finer due to the addition of elements such as titanium and manganese [16, 17]. On the other hand, the addition of cobalt to Cu–Al–Ni is reported to cause an increase in mechanical properties as well as the transformation temperature to the austenite phase, which means that this combination could be used at higher temperature [18]. Although it has quite good mechanical properties and corrosion resistance, Cu–Al–Ni is still less attractive compared to the widely used Ni–Ti, limiting its use. Saud et al. improved the mechanical properties of Cu–Al–Ni by adding quaternary elements, such as titanium, cobalt, and manganese, in various ratios as well as applying heat treatments to the alloys [16–18]. Even though this addition of Cobalt allows it to be used at higher temperatures, this fact alone does not guarantee its applicability. Since its applications would have to include actual use in corrosive environments, extensive study on the corrosion behavior of the Cu–Al–Ni shape memory alloys in such environments is needed. Moreover, in real applications, direct contact of Cu–Al–Ni with other metals would trigger galvanic corrosion. The latter indicates the need to study the corrosion behavior of Cu–Al–Ni-coupled low-carbon steel.

2 Methodology Procedure

2.1 Material Preparation, Homogenization, and Aging Treatment

The samples of Cu–Al–Ni were produced by melting high-purity metals, i.e., 99.999% copper, 99.999% aluminum, 99.95% nickel, and 99.8% cobalt, via an induction furnace, with the composition, as shown in Table 1. The compositions of the ternary (Cu–Al–Ni) and quaternary alloys (Cu–Al–Ni–xCo) were selected based on the compositions that provided optimal properties in our previous study [18]. The casting process was carried out with total weight of 500 g, see Table 1. These metals were melted in a silicon carbide crucible at a temperature of 1300 °C with continuous stirring and then poured into a cast iron mold with dimensions 270 mm × 50 mm × 20 mm. Since the as-cast microstructure is not normally uniform or homogenous, the homogenization was performed by heating the as-cast alloys to 900 °C for 30 min to obtain β phases. Quenching in a water medium to ensure the formation of martensite structures followed the homogenization. The samples were then preheated as an aging treatment in order to improve the functional properties of the Cu–Al–Ni shape memory alloys. The aging treatment was carried out in a laboratory muffle furnace with a resistance-embedded heating cell. In this setting, the test temperature was monitored by thermocouple, and the aging treatment was performed at 250 °C for 48 h. A summary of the entire heat-treatment procedure is presented in Fig. 1. The scratch-free and mirror-like surface of the samples produced after polishing was etched in order to create more contrast between the phases. Samples were etched using solution mixture of 2.5 g ($FeCl_3 \cdot 6H_2O$) and 48 ml methanol in 10 ml HCl for 20 s [19].

Table 1 Material weight for 500 g casting

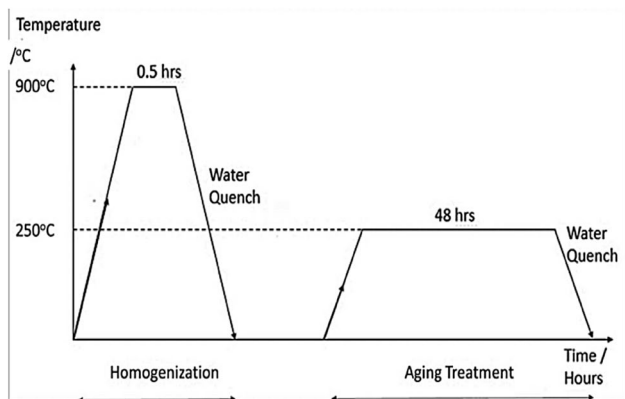| Alloy	Cu	Al	Ni	Co
Cu–Al–Ni	420.0	59.5	20.5	0
Cu–Al–Ni–0.4 wt% Co	418.4	59.5	20.0	2.1
Cu–Al–Ni–1.0 wt% Co	414.8	59.5	20.0	5.7

Fig. 1 Schematic of the heat-treatment profile

2.2 Compositional and Microstructural Characterization

The chemical composition of the cast alloys was determined by using inductively coupled plasma optical emission spectrometry (ICP-OES). An optical microscope (Olympus BX60F5) and field emission scanning electron microscope (FESEM, Zeiss-LEO Model 1530) with an accelerating voltage of 2–3 kV, coupled with energy dispersive x (EDX) facilities, were used to investigate the surface morphology of Cu–Al–Ni–xCo shape memory alloys. The X-ray diffraction analysis used in this research was done with a D5000 Siemens X-Ray diffractometer fitted with a CuKα X-ray source. The scanning mode was locked at 2θ range between 20° and 80°, and the scanning step set at 0.05°/s.

2.3 Sample Preparation for Electrochemical Test

The corrosion behavior and performance of the ternary (Cu–Al–Ni) with and without Co addition as ternary and quaternary alloys of Cu–Al–Ni, Cu–Al–Ni–0.4 wt% Co and Cu–Al–Ni–1.0 wt% Co were determined by using the Tafel electrochemical test. These sample were

electrochemically measured as uncoupled and coupled with low-carbon steel. The samples were prepared from the as-homogenized ingots, whereby the Cu–Al–Ni–xCo shape memory alloys ($x = 0$, 0.4, and 1 wt%) ingot were cut into small pieces of dimension 25 mm (L) × 20 mm (W) × 2 mm (t) to prepare for the electrochemical test. As for the low-carbon steel rebar, it was cut into 100 mm in length 5 mm in diameter. The coupled Cu–Al–Ni alloys/steel rebars were assembled by means of epoxy. Copper wires were also used to connect the Cu–Al–Ni–xCo shape memory alloys. The samples were drilled, and the copper wires were attached by means of nuts and bolts, as shown in Fig. 2a and b.

Electrochemical tests were conducted on the rectangular specimens, which had surface areas of 2.6 cm^2. The tests were conducted at 20 °C in open air in a glass cell containing 350 mL of 3.5% NaCl solution using a PARSTAT 2263 potentiostat/galvanostat (Princeton Applied Research). A three-electrode cell was used for potentiodynamic polarization tests, in which the reference electrode was a saturated calomel electrode (SCE). The counter electrode was made from a graphite rod, and the specimen was the working electrode. All experiments were carried out at a constant scan rate of 0.5 mV/s, which was initiated at −250 mV [vs. saturated calomel electrode (SCE)] below the open circuit potential. This fitting was inherently difficult; however, the software allows for manual control. Tafel fittings were generally carried out by selecting a segment of the curve from corrosion potential (φ_{corr}) and current density (I_{corr}), and subsequently estimated based on the value where the fit intercepted the potential value of the true corrosion potential (φcorr) [20]. Each experiment was repeated three times to check on the reproducibility of the results, and all potentials referred to the saturated calomel electrode (SCE), and the presented data are the average values with consideration of the standard deviation. The electrochemical setups for an uncoupled and a coupled specimen are, respectively, shown in Fig. 3a–c. The electrochemical tests were repeated three times.
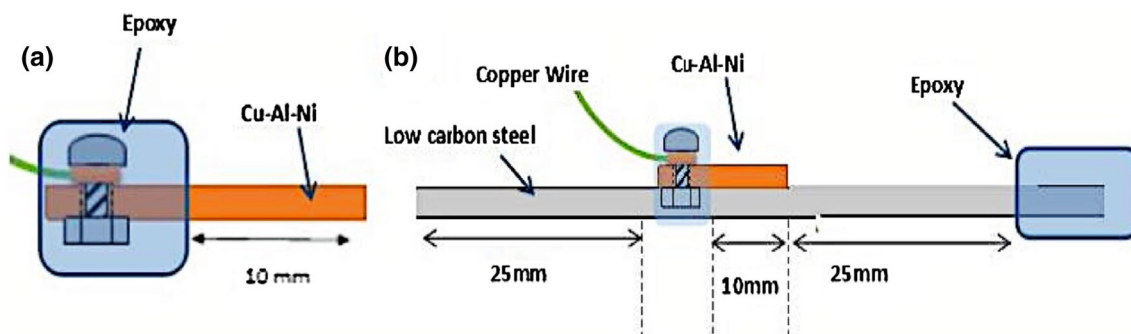

Fig. 2 Schematic **a** uncoupled Cu–Al–Ni, **b** coupled Cu–Al–Ni and low-carbon steel
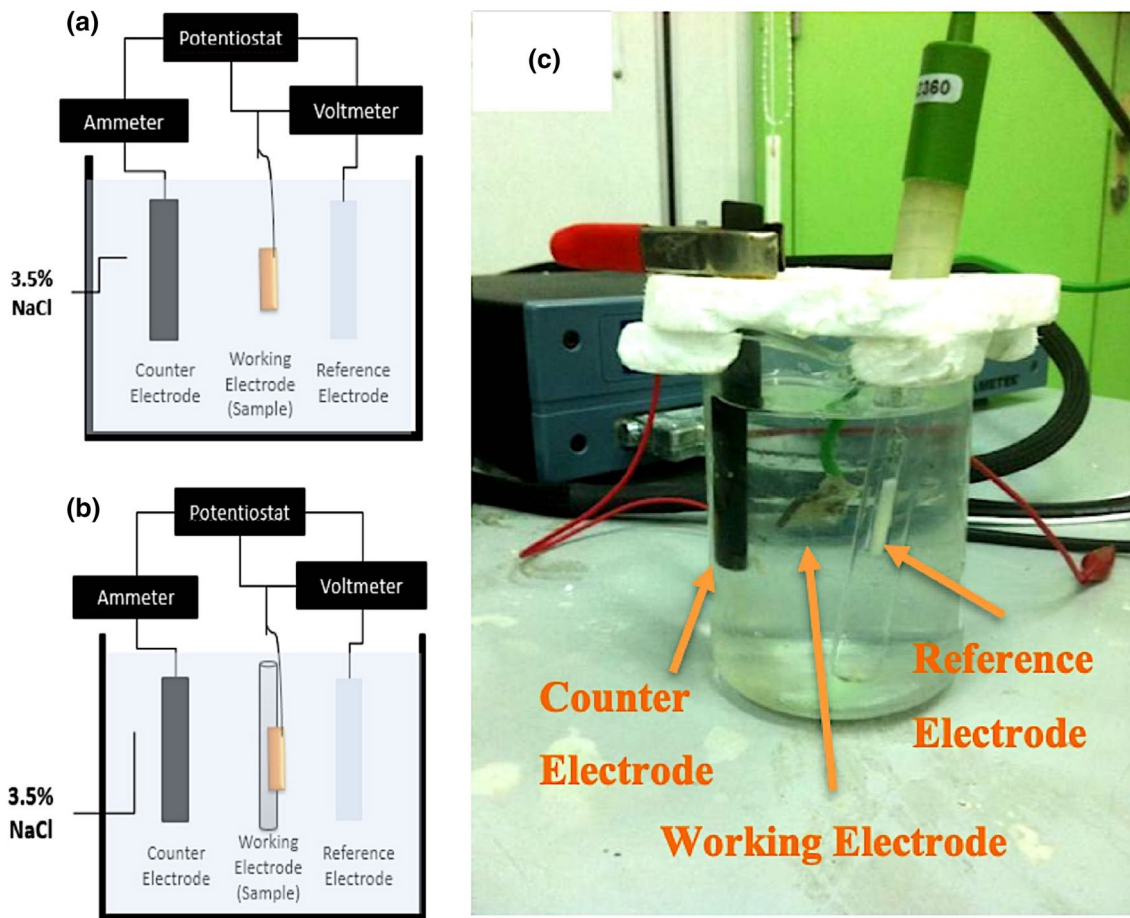
Fig. 3 Schematic of the electrochemical tests for **a** uncoupled, **b** coupled with low-carbon steel sample, and **c** experimental setups

Table 2 Inductively coupled plasma-optical emission spectrometry compositional analysis

Alloys	Composition (wt%)			
	Cu	Al	Ni	Co
Cu–Al–Ni	84.25	11.54	4.08	0
Cu–Al–Ni–0.4 wt% Co	80.02	11.87	4.95	0.27
Cu–Al–Ni–1.0 wt% Co	79.82	11.16	3.91	0.84

2.4 Vickers Microhardness Test

The microhardness of the specimens was measured via the Vickers hardness test (Shimadzu) using 10 kg force for 25 s. The average hardness of each specimen was attained from an average of three indentations with considered of the standard deviation.

3 Results and Discussion

3.1 Compositional Analysis of Cu–Al–Ni

The weight percentage of each element used based on a 500-g ingot melted during casting is shown Table 2. The inductively coupled plasma–optical emission spectrometry analysis shows almost similar results, with slight discrepancies due to equipment measurement inaccuracies.

3.2 Microstructural Analysis of Cu–Al–Ni–xCo Shape Memory Alloys

The microstructure micrographs and energy-dispersive X analysis of the homogenized Cu–Al–Ni shape memory alloys with and without modifications under aging treatment are shown in Fig. 4a–k. It is obvious that there are two distinct phases observed, namely, needle-like for β'_1 and plate-like for γ'_1. These two phases are also found in several other studies [14, 18, 21, 22]. Saud et al. [18] describe γ'_1 as having an 18R structure, while γ'_1 has a 2H structure. Similar to other

metals and alloys, the grain size of Cu–Al–Ni shape memory alloys increased with the aging treatment. It also could be seen that the thickness of the plate-like γ_1' increased, while the needle-like β_1' decreased after aging. No new phases or peaks were detected after aging treatment, and the X-ray diffraction results, Fig. 5a and b, also show no significant difference before and after aging, except that, after aging, the [128] peak was stronger; this result may be attributed to the coarsening of the martensite phase. On the other hand, the observed micrograph reveals that the grain size of the Cu–Al–Ni–*x*Co shape memory alloys became finer with the increasing cobalt content; in addition, a new phase, in the form of a precipitate, formed on the matrix. Saud et al. [18] point out that this phase is known as the γ_2 phase and consists of an intermetallic compound of $Al_{75}Co_{22}Ni_3$. This precipitate tended to segregate along the grain boundary, as presented in Fig. 4h, and also increased in size with higher cobalt content. This finding is also supported by energy-dispersive X analysis shown in Fig. 4k, when a high content of cobalt was detected in the precipitate. Similar to what occurred with Cu–Al–Ni without the cobalt addition, grain growth also occurred after the aging of Cu–Al–Ni–1.0 wt% Co shape memory alloys; however, there was a significant change in the microstructure of Cu–Al–Ni–1.0 wt% Co before and after aging treatment. Before aging, $Al_{75}Co_{22}Ni_3$ precipitates had a non-uniform size and distribution as shown in Figs. 4g and h for Cu–Al–Ni–0.4 w% Co and Cu–Al–Ni–1.0 wt% Co, respectively, where some of them were around 0.3 μm in diameter, while others had diameters of 0.1 μm only. After aging treatment, the small-sized precipitates had dissolved, leaving behind only the larger precipitates, which had reduced in size to around 0.25 μm. The dissolution and size reduction of $Al_{75}Co_{22}Ni_3$ precipitates also produced a significant impact on the X-ray diffraction results (see Fig. 5b), as, after aging, Cu–Al–Ni–1.0 wt% showed a reduction in its peaks' intensities. However, the peak for $Al_{75}Co_{22}Ni_3$ in Cu–Al–Ni–0.4 wt% increased after aging. This result may be due to the fact that the precipitate evolution was at the beginning stage for Cu–Al–Ni–0.4 wt% shape memory alloys.

3.3 Corrosion Performance

The polarization curves of the respective aged and unaged Cu–Al–Ni, coupled and uncoupled with the low-carbon steel rebar, obtained from electrochemical tests in 3.5% NaCl after 40 min of exposure, are shown in Figs. 6 and 7. The measured corrosion current density (I_{corr}), corrosion potential (Φ_{corr}, vs. SCE), cathodic Tafel slope (β_c), anodic Tafel slope (β_a), and corresponding corrosion rate (P_i) are determined and tabulated in Table 3. The coupled Cu–Al–Ni/low-carbon steel had a corrosion potential of − 313.78 mV, which lies in between the corrosion

potential of − 18.025 mV and − 422.521 mV for the isolated Cu–Al–Ni and low-carbon steel, respectively. However, the current density of the coupled material, which represents the corrosion rate, increased to 57.42 μA/cm^2, which exceeded those of both isolated materials, which were 19.231 μA/cm^2 and 28.592 μA/cm^2 for Cu–Al–Ni and low-carbon steel, respectively. This occurrence was due to the galvanic corrosion that took place when the two different metals were in contact. On the other hand, the aging treatment affected the corrosion behavior of the coupled Cu–Al–Ni/low-carbon steel significantly, i.e., the corrosion rate for Cu–Al–Ni decreased after aging treatment for the uncoupled as well as coupled samples, as presented in Fig. 6. This result could be related to the coarsening of the γ_1' phase after aging. Since the plate-like structure was Al-rich, the passive film of the surface perhaps became more stable, promoting a higher percentage of Al_2O_3 layers. Moreover, microscopically, the surface area was reduced, as needle-like β_1' decreased. Based on the presented results, it was also observed that the corrosion rate decreased with the increasing cobalt content. In other words, the corrosion resistance of Cu–Al–Ni was enhanced with cobalt addition. This fact may be related to the grain-size refinement caused by cobalt addition. Saud et al. [16, 17] also report a similar tendency as titanium and manganese were added, whereby an improvement in the corrosion resistance of the shape memory alloys was found to be due to the effects of the smaller grain size and higher volume fraction of the precipitates that enhanced the compactness and stability improvement of the passive film. The coupled samples also showed trends similar to those of the uncoupled samples. As a combination effect of aging and an alloying element addition, it was revealed that the Cu–Al–Ni–0.4 wt% Co also showed a decrease in corrosion rate after aging (see Fig. 7a), which may be attributed to microstructural changes. For instance, the precipitate volume fraction for Cu–Al–Ni–0.4 wt% Co was at the initiation stage; however, through aging, the fine-grain precipitates increased in density, reverting the sample to the X-ray diffraction results as shown in Fig. 5a and b. This evolution of the precipitates would enhance the compactness of and stability improvement made by the passive film. In addition, the improvement in corrosion resistance could also be related to the distribution and size of the precipitates. For Cu–Al–Ni–1.0 wt% Co SMA, for which precipitates were abundant, a decrease in the size and increase in the uniformity of the precipitates would improve the corrosion resistance, as displayed in Fig. 7b. Furthermore, the segregation of precipitates in a certain area, such as a grain boundary, would create a potential difference within the matrix. Thus, a more uniform anode–cathode distribution would reduce the localized galvanic corrosion between the precipitates and matrix,
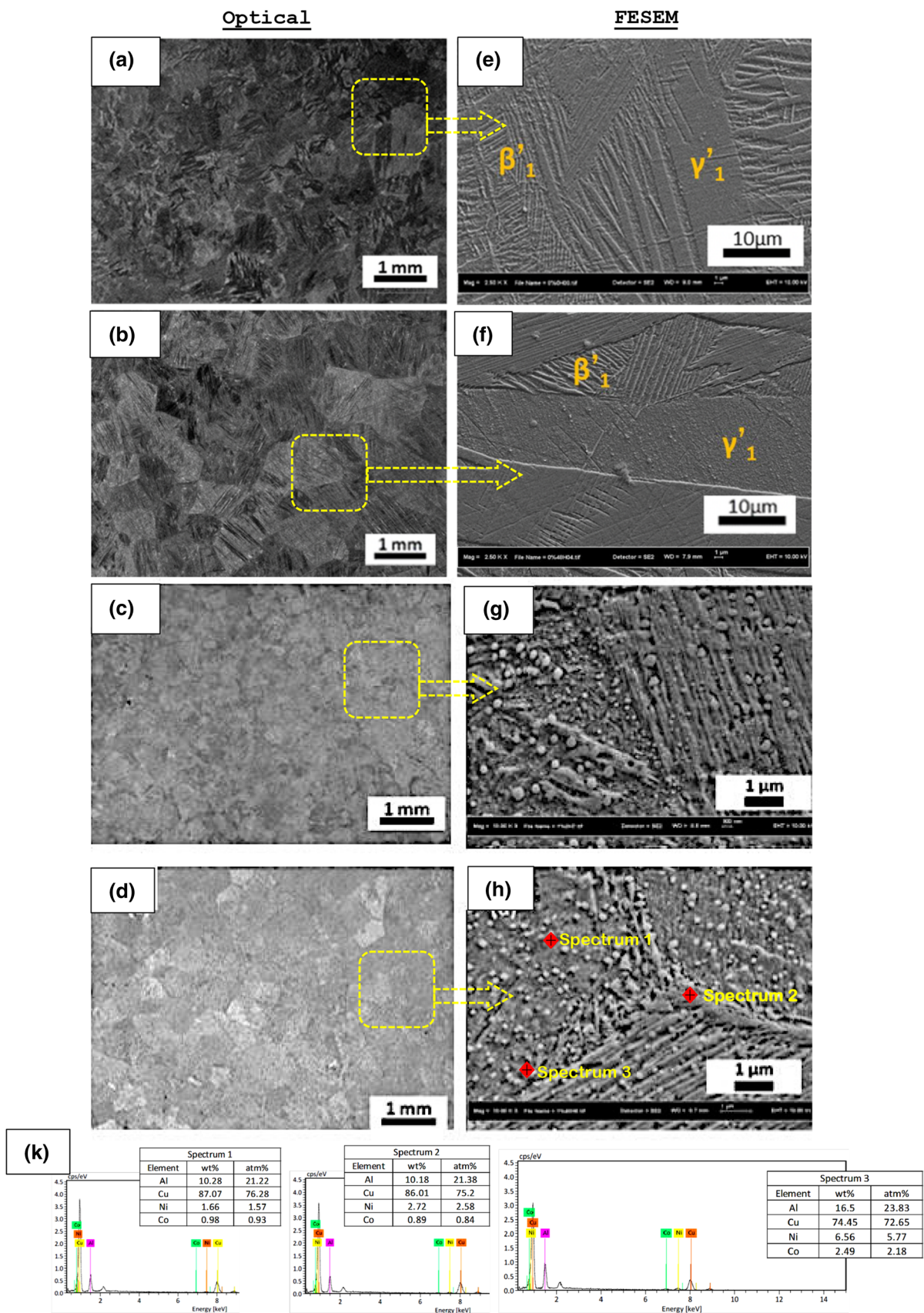
◄**Fig. 4** Optical and field emission electron microscopy images of **a**, **e** Cu–Al–Ni, **b**, **f** aged Cu–Al–Ni, **c** and **g** aged Cu–Al–Ni–0.4 wt% Co, **d**, **h** aged Cu–Al–Ni–1.0 wt% Co, and **k** energy dispersive X analysis

as evidenced from the micrographic variations presented in Fig. 4b–h. The coupled samples also followed the same trend as the isolated samples, whereby the corrosion rate decreased, but at a higher rate due to the galvanic effect.

3.4 Microhardness Analysis

The Vickers microhardness test was done to investigate the effects of cobalt addition and aging treatment on Cu–Al–Ni in terms of the hardness of each sample. The results of the Vickers microhardness test are shown in Table 4. The hardness increased proportionally with respect to Cobalt addition. This could be related to the quantity of precipitates that are formed. The existence of precipitates impedes dislocation, making the material become harder. This phenomenon is quite common in heat-treatable alloys, as they are being strengthened through precipitation hardening. Precipitation hardening usually becomes more effective after aging, as the precipitates can become more finely dispersed [23]. This could be evidently seen in Cu–Al–Ni–0.4 wt% Co and Cu–Al–Ni–1.0 wt% Co SMAs after the aging treatment.

4 Conclusions

Based on the results of the experimental work, the following conclusions have been drawn:

1. The addition of cobalt as the fourth element associated with the aging treatment of Cu–Al–Ni led to the promo-
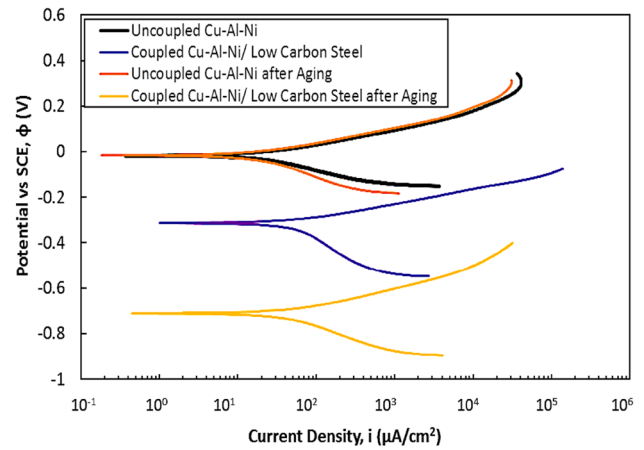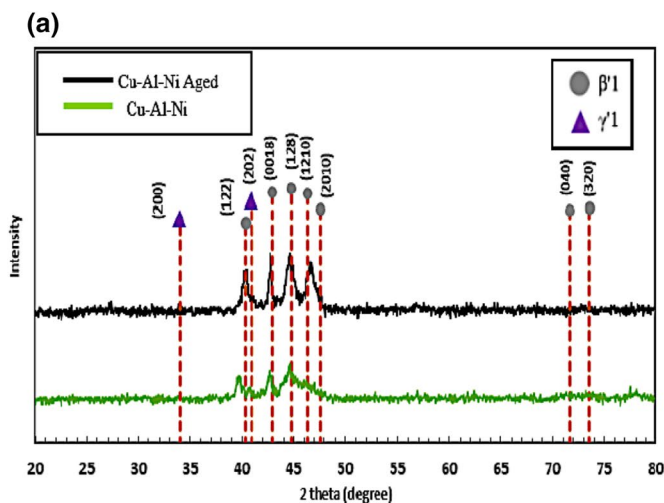

Fig. 6 Polarization curves of the electrochemical corrosion test of the coupled and uncoupled Cu–Al–Ni SMAs before and after aging

tion of the grain refinement and formed the precipitates of $Al_{75}Co_{22}Ni_3$ phase, which enhances the compactness in and the stability improvement brought by the passive film, and thus the corrosion resistance improved.

2. The best value of corrosion resistance of the coupled Cu–Al–Ni/low-carbon steel SMAs was obtained after having been modified with the addition of 1 wt% of Co along with the aging treatment, which resulted in 50% reduction in the corrosion rate compared with the uncoupled low-carbon steel sample.

3. The highest value for the microhardness of $340 \pm 17\ H_v$ for Cu–Al–Ni SMAs was obtained upon 1 wt% of Co addition and aging at 250 °C for 48 h.
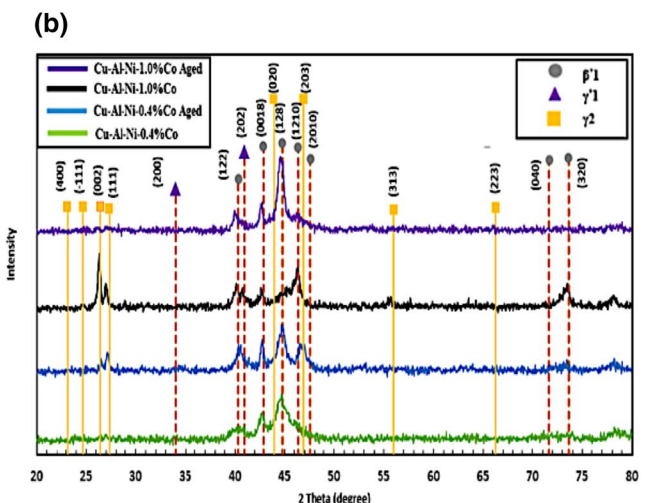

Fig. 5 X-ray diffraction patterns of the unaged and aged **a** Cu–Al–Ni SMAs and **b** Cu–Al–Ni–*x*Co SMAs
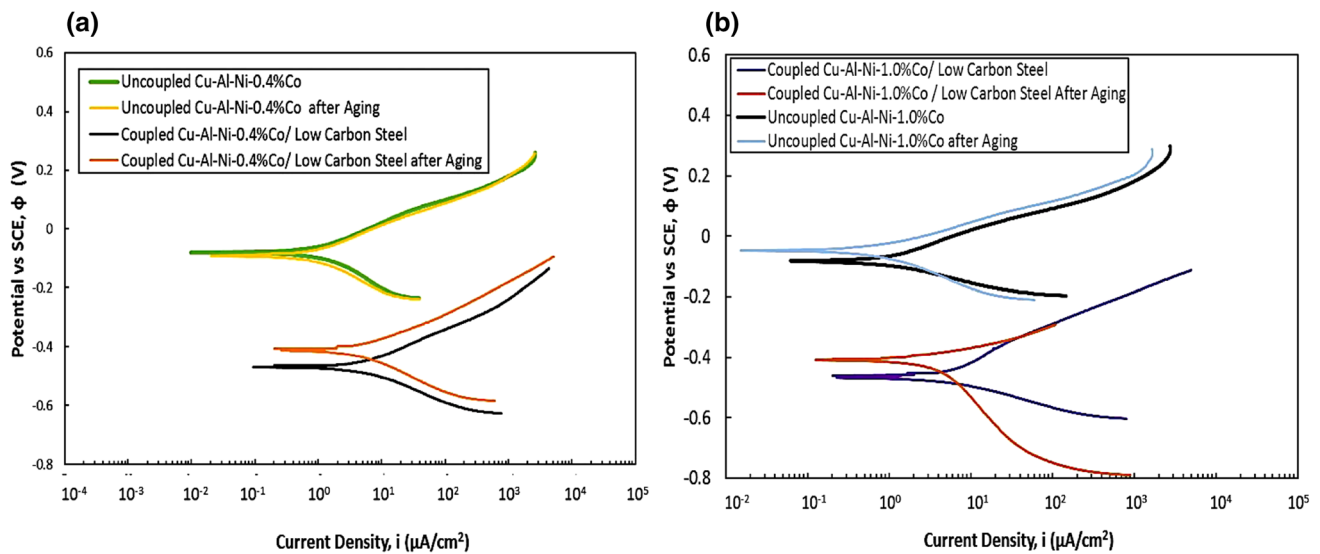
(a)

(b)

Fig. 7 Polarization curves of the electrochemical corrosion test of the coupled and uncoupled SMAs before and after aging: **a** Cu–Al–Ni–0.4 wt% Co SMAs and **b** Cu–Al–Ni–1.0 wt% Co SMAs

Table 3 Electrochemical test results

Alloys	φ_{corr} (vs. SCE) (mV)	I_{corr} ($\mu A.cm^{-2}$)	β_c (vs. SCE) (mV.decade^{-1})	β_a (vs. SCE) (mV.decade^{-1})	P_i mmpy
Uncoupled Cu–Al–Ni	-18.025 ± 0.9	19.231 ± 0.96	87.430 ± 4.37	63.969 ± 3.19	0.439 ± 0.02
Uncoupled aged Cu–Al–Ni	-14.48 ± 0.7	17.59 ± 0.87	127.52 ± 6.36	65.961 ± 3.29	0.402 ± 0.02
Uncoupled low-carbon steel	-422.521 ± 21.12	28.592 ± 1.42	88.608 ± 4.43	79.723 ± 3.98	1.102 ± 0.05
Coupled Cu–Al–Ni and low-carbon steel	-313.784 ± 15.6	57.421 ± 2.87	249.244 ± 12.46	66.595 ± 3.32	1.312 ± 0.06
Coupled aged Cu–Al–Ni and low-carbon steel	-712.904 ± 35.64	43.584 ± 2.1	136.001 ± 6.8	77.89 ± 3.89	0.995 ± 0.049
Uncoupled Cu–Al–Ni–0.4 wt% Co	-74.444 ± 3.72	13.717 ± 0.68	147.763 ± 7.38	108.869 ± 5.44	0.313 ± 0.015
Uncoupled aged Cu–Al–Ni–0.4 wt% Co	-88.993 ± 4.44	10.528 ± 0.52	128.204 ± 6.41	105.966 ± 5.23	0.241 ± 0.012
Uncoupled Cu–Al–Ni–1.0 wt% Co	-82.498 ± 4.12	10.478 ± 0.51	71.872 ± 3.54	105.046 ± 5.25	0.239 ± 0.011
Uncoupled aged Cu–Al–Ni–1.0 wt% Co	-46.841 ± 2.34	8.069 ± 0.4	115.165 ± 5.75	84.185 ± 4.2	0.184 ± 0.009
Coupled Cu–Al–Ni–0.4 wt% Co/low-carbon steel	-467.288 ± 23.3	54.994 ± 2.74	98.048 ± 4.9	104.688 ± 5.23	1.257 ± 0.062
Coupled aged Cu–Al–Ni–0.4 wt% Co/low-carbon steel	-411.799 ± 20.58	43.075 ± 2.15	104.726 ± 5.23	88.413 ± 4.42	0.984 ± 0.049
Coupled Cu–Al–Ni–1.0 wt% Co/low-carbon steel	-464.229 ± 23.11	51.994 ± 2.59	79.08 ± 3.95	149.155 ± 7.45	1.188 ± 0.059
Coupled aged Cu–Al–Ni–1.0 wt% Co/low-carbon steel	-406.431 ± 20.3	37.78 ± 1.88	297.709 ± 14.88	69.868 ± 3.49	0.663 ± 0.033

Table 4 Vickers microhardness test results

Samples	Vickers microhardness/H_v	
	Unaged	Aged
Cu–Al–Ni	245 ± 12.25	307 ± 15.35
Cu–Al–Ni–0.4 wt% Co	291 ± 14.55	335 ± 16.75
Cu–Al–Ni–1.0 wt% Co	301 ± 15.02	340 ± 17

5 Recommendations for Future Work

1. Current research covers the corrosion behavior of unmodified and modified Cu–Al–Ni coupled with low-carbon steel in 3.5% NaCl solution. Further studies on galvanic effect in concrete environment is needed to evaluate the application possibility in structures.
2. Further research maybe carried out with other alloying elements such as Zr, Sn, B, and others.
3. Aging parameters maybe varied to investigate the effects on corrosion behavior over a wide range of times and/or temperatures.

References

1. Schwartz M (2008) Smart materials. CRC Press, Boca Raton
2. Gandhi V, Thompson BS (1992) Smart materials and structures. Springer, London
3. Lagoudas DC (2008) Shape memory alloys: modeling and engineering applications. Springer, New York
4. Kumar P, Lagoudas D (2008) Introduction to shape memory alloys. Springer, Boston
5. Lagoudas DC (2008) Shape memory alloys and engineering applications. Springer, New York
6. Yildiz K, Kok M (2014) Study of martensite transformation and microstructural evolution of Cu–Al–Ni–Fe shape memory alloys. J Therm Anal Calorim 115:1509–1514
7. Nó ML, Caillard D, San Juan J (2009) A TEM study of martensite habit planes and orientation relationships in Cu–Al–Ni shape memory alloys using a fast Δg-based method. Acta Mater 57(4):1004–1014
8. Otsuka K, Wayman CM (1999) Shape memory materials. Cambridge University Press, Cambridge
9. Wu S, Lin H (2000) Recent development of TiNi-based shape memory alloys in Taiwan. Mater Chem Phys 64(2):81–92
10. Duerig TW, Melton KN, Stockel D, Wayman CM (1990) Engineering aspects of shape memory alloys, Books on Demand. Butterworth Heinemann Publishing, London
11. Lopez GA, Barrado M, Bocanegra EH, San Juan JM, No ML (2010) Cu–Al–Ni shape memory alloy composites with very high damping capacity. In: International conference on martensitic transformations (ICOMAT). John Wiley & Sons, Inc., Hoboken, NJ, USA, pp 231–238
12. Song G, Patil D, Kocurek C, Bartos J (2010) Earth and space 2010: engineering, science, construction, and operations in challenging environments. ASCE Publications, League City, pp 1551–1567
13. Schüssler A, Exner H (1993) The corrosion of nickel-aluminium bronzes in seawater—I. Protective layer formation and the passivation mechanism. Corros Sci 34(11):1793–1802
14. Suresh N, Ramamurty U (2008) Aging response and its effect on the functional properties of Cu–Al–Ni shape memory alloys. J Alloys Compds 449(1–2):113–118
15. Lee JS, Wayman CM (1986) Grain refinement of a Cu–Al–Ni shape memory alloy by Ti and Zr additions. Trans Japan Inst Met 27(8):584–591
16. Saud S, Hamzah E, Abubakar T, Zamri M, Tanemura M (2014) Influence of Ti additions on the martensitic phase transformation and mechanical properties of Cu–Al–Ni shape memory alloys. J Therm Anal Calorim 1:111–122
17. Saud S, Hamzah E, Abubakar T, Bakhsheshi-Rad HR, Zamri M, Tanemura M (2014) Effects of Mn additions on the structure, mechanical properties, and corrosion behavior of Cu-Al-Ni shape memory alloys. J Mater Eng Perform 11:3620–3629
18. Saud S, Hamzah E, Abubakar T, Bakhsheshi-Rad HR (2015) Thermal aging behavior in Cu–Al–Ni–xCo shape memory alloys. J Therm Anal Calorim 119(2):1273–1284
19. Chang SH (2011) Influence of chemical composition on the damping characteristics of Cu–Al–Ni shape memory alloys. Mater Chem Phys 125(3):358–363
20. Sudholz A, Gusieva K, Chen X, Muddle B, Gibson M, Birbilis N (2011) Electrochemical behaviour and corrosion of Mg–Y alloys. Corros Sci 53(6):2277–2282
21. Recartea V, Pérez-Sáeza RB, Bocanegrac EH, Nóc ML, San Juan J (1999) Dependence of the martensitic transformation characteristics on concentration in Cu–Al–Ni shape memory alloys. Mater Sci Eng A 273–275:380–384
22. Sakamoto H, Shimizu KI (1989) Effect of heat treatments on thermally formed martensite phases in monocrystalline Cu–Al–Ni shape memory alloy. ISIJ Int 29(5):395–404
23. Callister WD, Rethwisch DG (2011) Materials science and engineering. Wiley, New York

Publisher's Note Springer Nature remains neutral with regard to jurisdictional claims in published maps and institutional affiliations.